Surface polaritons and attenuated total reflection spectra of layered antiferromagnets in the Faraday configuration

1995 J. Phys.: Condens. Matter 7 6423

(http://iopscience.iop.org/0953-8984/7/32/008)

J. Phys.: Condens. Matter 7 (1995) 6423–6436. Printed in the UK

Surface polaritons and attenuated total reflection spectra of layered antiferromagnets in the Faraday configuration

Kamsul Abraha†‡, S R P Smith† and D R Tilley†§

† Department of Physics, University of Essex, Colchester CO4 3SQ, UK
‡ Jurusan Fisika FMIPA, Universitas Gadjah Mada, Yogyakarta 55281, Indonesia
§ School of Physics, Universiti Sains Malaysia, 11800 USM Penang, Malaysia

Received 27 March 1995

Abstract. A detailed theoretical discussion is presented for the surface polaritons and attenuated total reflection (ATR) spectra of layered antiferromagnets when an applied magnetic field is parallel to the surface and to the propagation direction (i.e. Faraday geometry). Our numerical results for NiO reveal the existence of both bona fide surface polariton and generalized surface modes which were never indicated before in magnetic systems. In addition, the conventional derivation of the rf permeability tensor μ has recently been argued to be incorrect and consequently should be replaced by an alternative derivation that is consistent with macroscopic electrodynamics. We suggest, in view of previous experience on FIR magnetic spectroscopy, that FIR ATR spectroscopy may directly discriminate between the alternative forms for μ. The results are equally valid for a large class of magnetic layered systems including artificial magnetic superlattices with antiferromagnetic coupling.

1. Introduction

A recent study of the theoretical and experimental oblique incidence reflectivity of the uniaxial antiferromagnet FeF_2 [1, 2] has shown that very high-quality spectra of magnetic excitations in the retarded (electromagnetic) region $q \sim \omega/c$ can be obtained with a high-resolution far-infrared (FIR) spectrometer. The measured spectra are governed by the frequency-dependent magnetic permeability tensor $\mu(\omega)$, which represents the response of the spin system to a driving electromagnetic field at FIR frequency ω. In the conventional theory the linear response of the system to an applied rf field $\boldsymbol{h}\exp(-i\omega t)$ is used as the basis for the susceptibility or permeability calculation in a magnetic crystal [3]. However, it has recently been argued [4] that this is incorrect for layered antiferromagnets such as NiO, as well as for a large class of easy plane magnetic systems including artificial magnetic superlattices with some degree of antiferromagnetic coupling in which successive spin layers order as in figure 1. The alternative method, which we refer to as the h/b method, proposes that the correct response consistent with macroscopic electrodynamics involves the components of $\boldsymbol{h}$ parallel to the layers but the components of $\boldsymbol{b}$ normal to the layers. This approach is in accordance with the effective medium theory of magnetic superlattices [5, 6] in that these are the components that are continuous from layer to layer. Such a calculation leads to a shifted resonance in the permeability tensor component $\mu_{zz}(\omega)$ which incorporates effects from demagnetizing fields that are not present in permeabilities calculated using the conventional or constant-h method. For future reference, the resonance

0953-8984/95/326423+14$19.50

frequencies ω_- obtained by the conventional method and ω_d obtained by the h/b method are given by

$$\omega_- = \gamma(2H_eH_a\sin^2\theta)^{1/2} \tag{1}$$

and

$$\omega_d = \gamma[2H_e(H_a + 4\pi M_s)\sin^2\theta]^{1/2}. \tag{2}$$

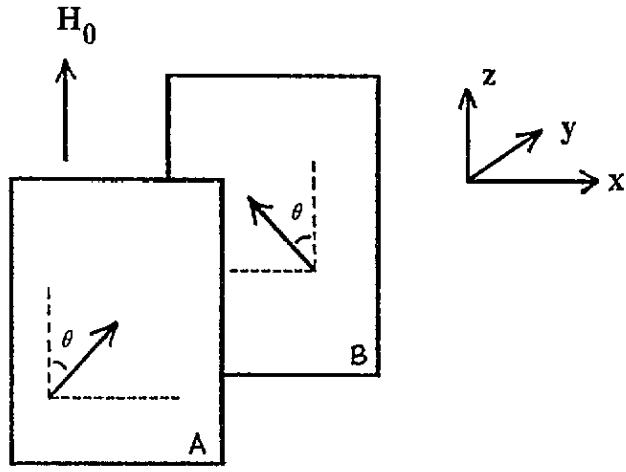

Figure 1. Magnetic moment arrangement in layered antiferromagnet NiO. The aligned spins in layer A are antiferromagnetically coupled to the spins in layer B. In the absence of the external field H_0 moments on neighbouring planes are ordered antiparallel along x direction. In the presence of a field the spins in each layer make an angle θ with respect to H_0 [4, 9].

Here H_e is the exchange field, H_a is an effective anisotropy field, M_s is the saturation magnetization of each magnetic sublattice and θ is the canting angle shown in figure 1. For bulk crystals, $\cos\theta = H_0/2H_e$. The other components $\mu_{xx}(\omega)$, $\mu_{xy}(\omega)$ and $\mu_{yy}(\omega)$ in both methods take the same form [4] with a single resonance frequency in an applied field H_0 given by

$$\omega_+ = \gamma(H_0^2 + H_0H_a\cos\theta)^{1/2}. \tag{3}$$

If substantiated by experiment, [4] will lead to a substantial reconsideration of a number of established results for a large class of magnetic layered structures, including easy plane antiferromagnets and rare earth magnets with helical magnetic orderings [7, 8]. *The main question that should be addressed is how the difference between the two expressions for μ_{zz} can be justified experimentally.* In the light of its importance, theoretical discussion of this question is a very desirable preliminary to experimental studies. Calculations of the kind presented here and previously [9] are also timely since FIR spectroscopy of magnetic materials at high resolution is now available [1, 2].

In a previous paper [9] we have presented a theoretical discussion of the surface polaritons and ATR spectra of layered antiferromagnets in the Voigt geometry (in which the applied field is parallel to the interface and perpendicular to the propagation direction) with particular reference to NiO (Néel temperature $T_N = 523$ K). It has the type II fcc structure at $T < T_N$, with ferromagnetic layers of spins in (111) planes stacked antiferromagnetically along ⟨111⟩ directions [10]. With a magnetic field H_0 applied parallel to the easy planes, the equilibrium orientation of the sublattice moments is as shown in figure 1. We find

that the solutions for the dispersion relations of surface polaritons in the Voigt geometry separate into s (TE) and p (TM) polarization [9] using the usual nomenclature [1, 2]. The s polarization solution involves only the tensor components μ_{xx}, μ_{xy} and μ_{yy}, and does not directly resolve the question. Surprisingly, for the p polarization solution, which involves only μ_{zz}, we find no surface polariton modes. Therefore experiments aimed specifically at the surface polaritons in this configuration cannot resolve the question either.

In this paper we continue and extend the work considerably for the other geometry of fundamental interest in which the applied field is parallel to the interface and to the direction of propagation, also known as the Faraday geometry. We find that the required dispersion relation for surface polaritons now involves all the four tensor components μ_{xx}, μ_{xy}, μ_{yy} and μ_{zz}. For the particular case of NiO we find both *bona fide surface polariton and generalized surface modes* [11] which correspond to two-component surface waves decaying away from the interface. Particularly, both components decay exponentially in the surface polariton modes and decay in an oscillatory fashion in the generalized surface modes. These modes clearly display the shifted resonance in μ_{zz}; that is, the resonance frequencies ω_- obtained by the conventional method and ω_- obtained by the h/b method are markedly separated in the ω–q plane. Accordingly, it is a plausible speculation that the question of the correct form of μ can be resolved conclusively by FIR ATR spectroscopy which gives direct access to the surface polaritons. We believe that this article represents a significant extension of our previous work in [9]. As far as we are aware, there have been no previous publications which deal with ATR spectra of surface magnetic polaritons in the Faraday geometry.

In the next section we derive and discuss the surface polariton dispersion curves in the Faraday configuration. In section 3 we then derive and show ATR spectra. Calculations are presented and illustrated numerically using the experimental magnetic parameters of NiO already quoted in [9]. We finally present a general discussion and conclusions of this paper in section 4.

2. Surface magnetic polaritons

With the system of coordinates shown in figure 1, we examine surface polaritons at the interface $y = 0$ between vacuum ($y < 0$) and the magnetic medium ($y > 0$) following the usual procedure [3]. Elimination of the electric field variables from Maxwell's equations gives the required equation for the rf field $\boldsymbol{H}$:

$$\nabla^2 \boldsymbol{H} - \nabla(\nabla \cdot \boldsymbol{H}) - (\varepsilon/c^2)\mu \cdot \partial^2 \boldsymbol{H}/\partial t^2 = 0. \tag{4}$$

The surface polariton fields, with amplitudes that decay with distance from the interface and propagating parallel to the applied field H_0 as a plane wave in the z direction, can be written

$$\boldsymbol{H} = (H_x^0, H_y^0, H_z^0)\exp(\alpha_0 y)\exp(\mathrm{i}qz - \mathrm{i}\omega t) \qquad (y < 0) \tag{5}$$

$$\boldsymbol{H} = (H_x, H_y, H_z)\exp(-\alpha y)\exp(\mathrm{i}qz - \mathrm{i}\omega t) \qquad (y > 0) \tag{6}$$

where q is the wave vector of the surface polaritons and α_0 and α are the spatial decay constants in vacuum and the medium of dielectric constant ε, respectively. It can be shown that the decay constant α_0 is simply given by

$$\alpha_0^2 = q^2 - \omega^2/c^2. \tag{7}$$

After substituting equation (6) into equation (4) and using the explicit form of μ already quoted in [9], we have a set of three homogeneous linear equations for the components H_x, H_y and H_z:

$$\begin{bmatrix} \alpha^2 - q^2 + \varepsilon\mu_{xx}\omega^2/c^2 & \varepsilon\mu_{xy}\omega^2/c^2 & 0 \\ -\varepsilon\mu_{xy}\omega^2/c^2 & \varepsilon\mu_{yy}\omega^2/c^2 - q^2 & iq\alpha \\ 0 & iq\alpha & \alpha^2 + \varepsilon\mu_{zz}\omega^2/c^2 \end{bmatrix} \begin{bmatrix} H_x \\ H_y \\ H_z \end{bmatrix} = 0. \tag{8}$$

As seen from (8), the polarization of the surface modes is neither transverse electric (TE) nor transverse magnetic (TM) since the electric and magnetic vectors do not lie in the sagittal plane, i.e. the plane defined by the normal of the interface and the propagation direction. The electric vector, for instance, traces out an ellipse which contains the wave vector q and is inclined to the sagittal plane. *Consequently, a combination of s and p polarized incident light is necessary in order to excite the surface modes by optical techniques such as ATR.* This is indeed the case as will be made clear in section 3.

In order for equation (8) to have a nontrivial solution, the determinant of coefficients must vanish. As a result, the spatial decay constant α is then given by

$$\alpha^4 + A\alpha^2 + B = 0 \tag{9}$$

where

$$A = \frac{\omega^2}{c^2}\varepsilon(\mu_{xx} + \mu_{zz} + \mu_{xy}^2/\mu_{yy}) - (1 + \mu_{zz}/\mu_{yy})q^2 \tag{10}$$

and

$$B = \frac{\mu_{zz}}{\mu_{yy}}\left[q^4 - q^2\frac{\omega^2}{c^2}\varepsilon(\mu_{xx} + \mu_{yy}) + \left(\frac{\omega^2}{c^2}\varepsilon\right)^2(\mu_{xx}\mu_{yy} + \mu_{xy}^2)\right]. \tag{11}$$

Of the four roots in (9), only the two positive or those with positive real parts are suitable for exponentially decaying waves in the magnetic medium [11]. If we call these roots α_1 and α_2 for a given ω and q, then there are two possible surface modes corresponding to the following conditions: (i) bona fide or standard surface modes if α_1 and α_2 are both real and positive, and (ii) generalized surface modes if α_1 and α_2 are mutually complex conjugates with positive real parts. If α_1 is real and α_2 is pure imaginary, or vice versa, we have pseudosurface modes which are not true surface modes. It is clear from (9) that the medium is birefringent, that is there are two acceptable values of the wave vector q for a given frequency ω and each mode has a well defined polarization [12]. With two decay constants α_1 and α_2, the surface polariton fields inside the sample ($y > 0$) can be written as a linear superposition of two plane waves such as (6):

$$\boldsymbol{H} = \left[\sum_{i=1}^{2}(H_x^{(i)}, H_y^{(i)}, H_z^{(i)})\exp(-\alpha_i y)\right]\exp(iqz - i\omega t). \tag{12}$$

It should be noted that only two independent field amplitudes or coefficients in (12) are needed, for example $H_z^{(1)}$ and $H_z^{(2)}$, since the polarization of each term here is definite and therefore all the other field components can be determined once an unknown one has been chosen. The expression (5) for $\boldsymbol{H}$ in vacuum, on the other hand, describes a running surface wave in an isotropic medium. In this case, the polarization is not definite so there are also two independent field amplitudes (for instance, H_x^0 and H_z^0). Finally, H_y^0 and all the remaining components of $\boldsymbol{H}$ written in (5) and (6) can be found from Maxwell's equations.

The required dispersion relation for the surface polaritons can be obtained by applying the electromagnetic boundary conditions at the interface $y = 0$ for the parallel components E_x, E_z, H_x and H_z. As mentioned before, we should first express these in terms of the four

unknowns H_x^0, H_z^0, $H_z^{(1)}$ and $H_z^{(2)}$. The boundary conditions immediately give the implicit dispersion relation in the Faraday configuration

$$\mu_{zz}\alpha_0[\alpha_1^2+\alpha_2^2+\alpha_1\alpha_2+\varepsilon\alpha_0(\alpha_1+\alpha_2)+\frac{\omega^2}{c^2}\varepsilon(\mu_{zz}-\varepsilon)]$$
$$+\alpha_1\alpha_2(\varepsilon\alpha_0+\alpha_1+\alpha_2)-\alpha_0 q^2\mu_{zz}(\mu_{zz}-\varepsilon)/\mu_{yy}=0. \tag{13}$$

It is worth pointing out that the algebra has involved cancelling out a factor $(\alpha_1-\alpha_2)$, which is consistent with the assumption (12) that a solution to equation (4) in the sample is the superposition of the two waves associated with the two different decay constants. In other words, two such waves are required to satisfy the electromagnetic boundary conditions at the interface [11].

As evident from equations (9)–(11) and (13), all the tensor components μ_{xx}, μ_{xy} and μ_{yy}, as well as μ_{zz} in question, appear in the dispersion relation for the surface polaritons. In contrast to our previous results [9] for the Voigt geometry, which showed the nonexistence of the p polarized surface modes, the relation (13) would certainly provide a direct experimental probe of the surface polaritons that can in principle discriminate between the alternative expressions for μ_{zz} by analysing the corresponding ATR spectra. In section 3, we will calculate and discuss some ATR curves for surface polaritons of NiO in the Faraday geometry that clearly highlight the potential of this technique to resolve the question.

In equations (10), (11) and (13), q appears only as even powers so that the dispersion curves for positive and negative q are identical. That is, changing the sign of q does not change the frequency ω : $\omega(-q)=\omega(q)$. The surface mode propagation is therefore reciprocal, which is required by symmetry [13]. With $\alpha=0$ or $B=0$ in (9), we obtain the dispersion relation for the bulk modes which is again even in q so the bulk mode propagation is also reciprocal.

In the nonretarded limit $q \gg \omega/c$ $(c\to\infty)$, the decay constants are $\alpha_1\to q$ and $\alpha_2\to q(\mu_{zz}/\mu_{yy})^{1/2}$ so that equation (13) reduces to

$$\mu_{zz}^{-1}(\mu_{yy}\mu_{zz})^{1/2}=-1. \tag{14}$$

Consequently, a bona fide surface wave will only exist in this limit if both μ_{yy} and μ_{zz} are negative in the frequency region of interest.

Equation (13) together with equations (7) and (9) has been solved numerically for the dispersion curves of NiO after making use of the magnetic permeability tensor derived in the conventional and the h/b methods. Typical results for bulk and surface polaritons are shown in figure 2 with the applied field $H_0=0$ and in figure 3 with $H_0=3$ T. Here we plot the results with μ_{zz} derived from the conventional analysis in figures 2(a) and 3(a) and from the h/b analysis in figures 2(b) and 3(b). In all cases, each of the dispersion curves starts as a bona fide surface mode at a certain point on a boundary of one bulk continuum, then continues as a generalized surface mode over a narrow range of q and finally terminates as another bona fide surface mode at a finite value of q in the other bulk continuum.

Figures 2 and 3 also show that the surface modes in the Faraday geometry have no magnetostatic limits $q \gg \omega/c$ in the sense that they exist only over a finite range of q, so they actually resemble the virtual surface modes [3, 11]. As revealed by further numerical exploration, this occurs since the values of μ_{yy} and μ_{zz} in the frequency interval occupied by the surface polariton curves do not satisfy the condition required by equation (14). We should also emphasize at this point that both sets of curves, as shown in figure 2 or 3, clearly display the shifted resonance in μ_{zz}. That is, the resonance frequencies ω_- obtained by the conventional method and ω_d obtained by the h/b method are markedly separated in the ω–q plane. We may then expect that an ATR measurement will be able to

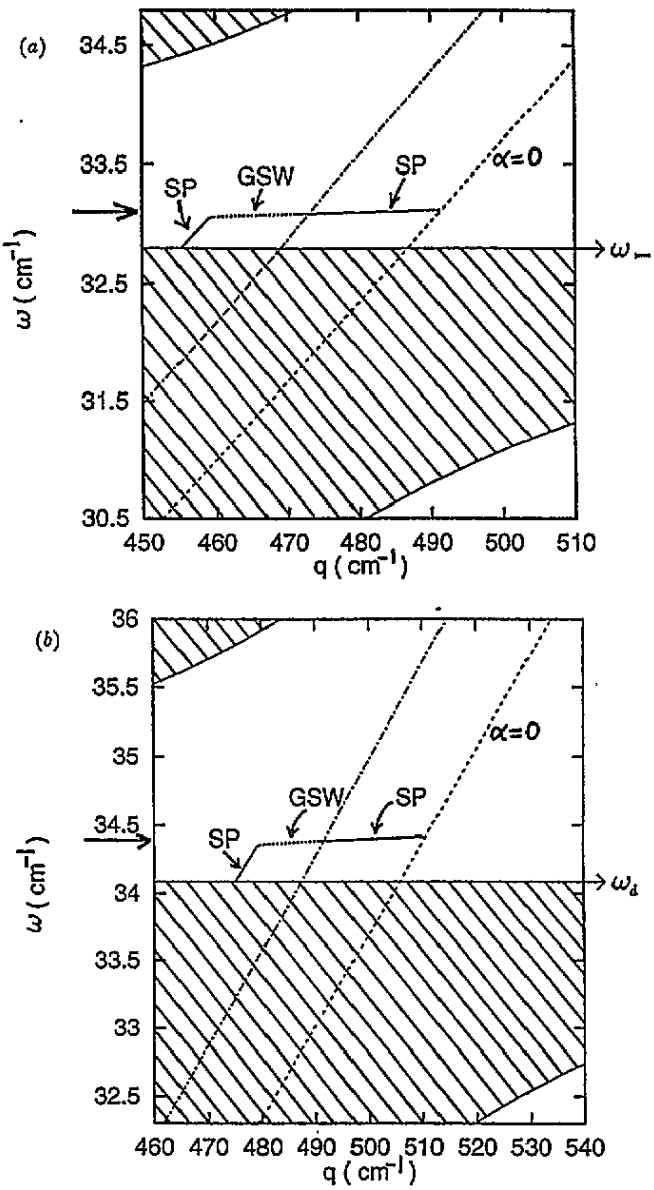

Figure 2. The dispersion curves for bona fide surface polaritons (SP, solid lines) and generalized surface waves (GSW, dotted lines) for NiO in the Faraday geometry in zero applied field: (a) conventional method, (b) h/b method. The shaded regions and the dashed curve $\alpha = 0$ are bulk polariton dispersion curves. In both sets of curves, the ATR scan line (dashed-dotted lines) is drawn for $\phi = 42°$ and $\varepsilon_p = 11.56$ (Si). The arrows on the vertical axis indicate frequencies where the ATR scan line crosses a surface polariton dispersion curve. The resonance frequencies ω_- and ω_d are given by (1) and (2), respectively.

discriminate the difference. For future reference, we also plot the ATR scan line specified by $q = \varepsilon_p^{1/2}(\omega/c)\sin\phi$ with the prism dielectric constant $\varepsilon_p = 11.56$ (Si) and the fixed angle of incidence in the prism $\phi = 42°$. As indicated by the arrows in the figures, ATR dips may be expected when the scan lines cross the surface polariton curves. This is the

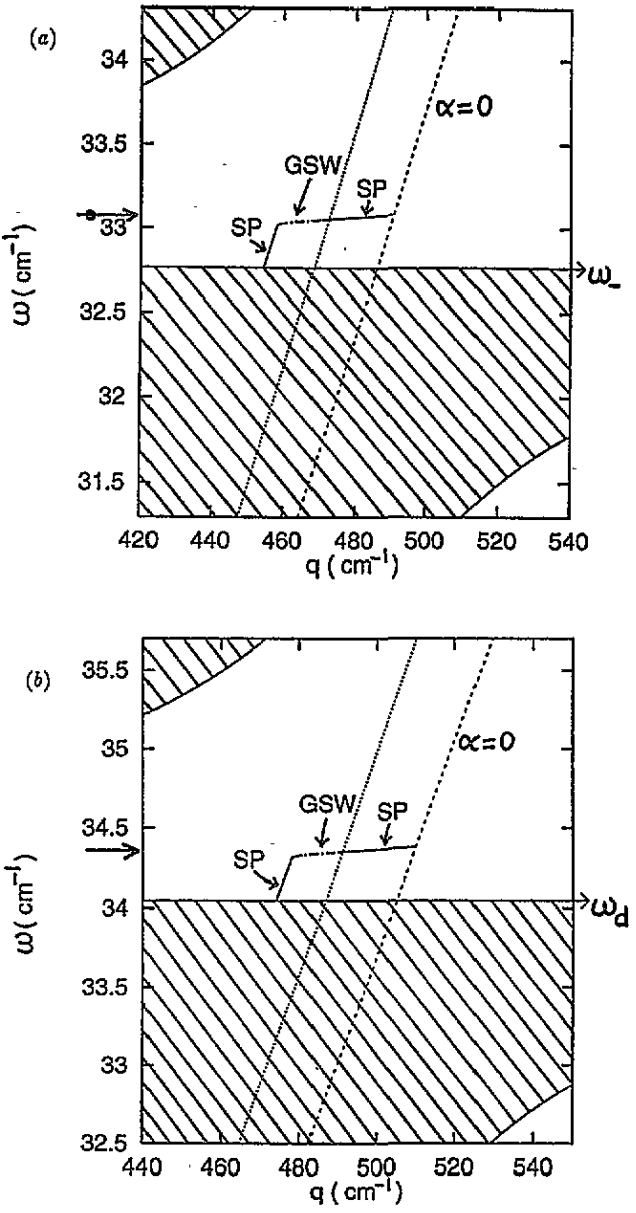

Figure 3. The dispersion curves for surface polaritons and generalized surface waves for NiO in the Faraday geometry in applied field $H_0 = 3$ T. Other details as in figure 2. Frequencies of ATR dips discussed later in section 3 are indicated by the arrows on the vertical axis.

case as will be made clear in section 3.

In figure 4, the reduced decay constants α_i/q in the magnetic crystal are plotted against the wave vector q of the surface polaritons with dispersion curves shown in figure 3. The real and imaginary parts of the complex conjugate quantities α_1 and α_2 are also plotted in the generalized surface wave regions. We see that one of the decay constants goes to zero at the endpoints of the surface polariton curves, which means that near these points

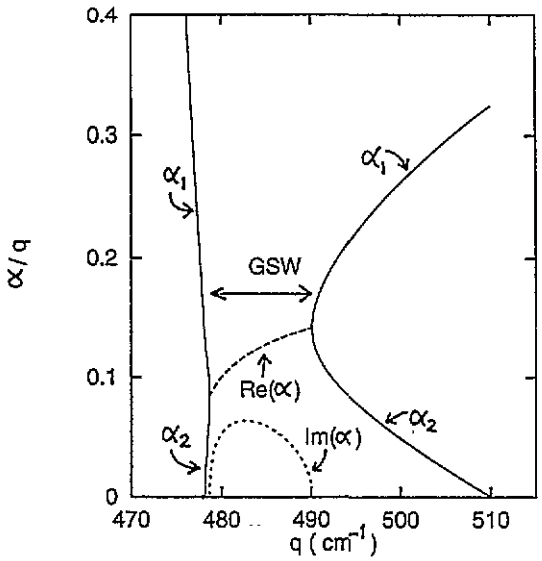

Figure 4. The reduced decay constants (α/q) in the sample versus wave vector q of surface polaritons whose dispersion curves are shown in figure 3(b). In the generalized surface wave (GSW) regions, the real and imaginary parts of α are also plotted.

only the solution involving one α is necessary. In other words, the influence of the crystal birefringence on the surface modes in this configuration will disappear as they merge with the bulk modes. A similar phenomenon was also found for surface magnetoplasmons of a semiconductor in an appropriate geometry [11, 14].

3. Calculations of the attenuated total reflection (ATR)

As indicated in section 2, the surface polariton modes can couple to both s and p polarized light in an ATR experiment due to the complicated polarization of the surface mode electromagnetic fields. In view of this feature, we will consider an ATR arrangement in the Otto configuration as illustrated in figure 5 which takes into account all the four possible polarization geometries for the incident and reflected light [2, 14]: s to s, s to p, p to p and p to s reflection. Since the derivation of the expressions for the reflectivity involves a sequence of steps familiar from ordinary optics, we need only give an outline of the procedure.

As shown in figure 5, we consider a three-layer system consisting of prism, air gap and magnetic sample. We choose the y axis normal to the interfaces and the yz plane as the plane of incidence; the air gap extends from $y = -d$ to $y = 0$. The applied magnetic field H_0 is along the z axis.

Consider first an s polarized incident wave of frequency ω and wave vector $\boldsymbol{k} = (0, k_\perp, k_\parallel)$ on the $y = -d$ interface; with $k_\parallel = k\sin\phi$, $k_\perp = k\cos\phi$, $k = \varepsilon_p^{1/2}(\omega/c)$ and ϕ the angle of incidence. The electric and magnetic fields are given by $(E_0, 0, 0)$ and $(E_0/\mu_0\omega)$ $(0, k_\parallel, -k_\perp)$, respectively, with the same phase factor of the form $\exp(\mathrm{i}(k_\perp y + k_\parallel z - \omega t))$.

Up to this point, it is useful to calculate the electric and magnetic field components of the wave propagating in the magnetic sample with wave vector $\boldsymbol{k}_s = k[0, (k_s^2/k^2 - \sin^2\phi)^{1/2}, \sin\phi]$. This wave satisfies the wave equation (4), so the magnitude of $\boldsymbol{k}_s$ can be

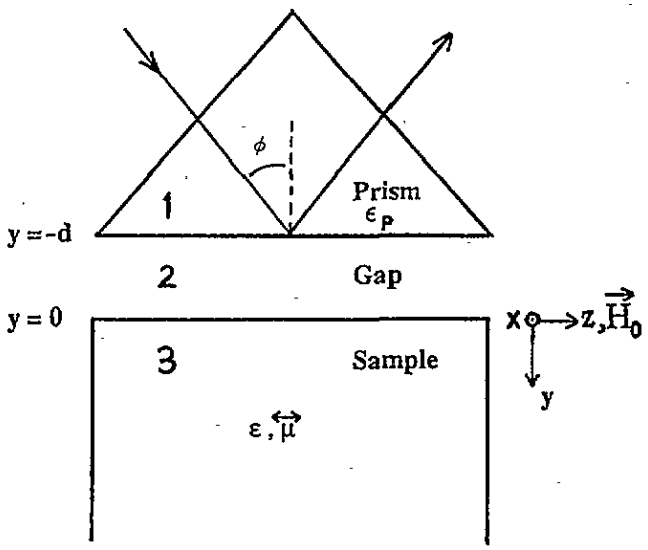

Figure 5. The geometry for the ATR calculation. The incident light of frequency ω in the prism of dielectric constant ε_p propagates at an angle $\phi > \phi_c$, with $\phi_c = \sin^{-1}(1/\varepsilon_p^{1/2})$ the critical angle for total internal reflection. The external magnetic field H_0 is in the plane of incidence.

obtained from the quadratic equation in k_s^2

$$k_s^4 + Ck_s^2 + D = 0 \tag{15}$$

where

$$C = -(\mu_{xx} + \mu_{zz} + \mu_{xy}^2/\mu_{yy})q_0^2 - (1 - \mu_{zz}/\mu_{yy})k^2 \sin^2\phi \tag{16}$$

and

$$D = q_0^4\mu_{zz}(\mu_{xx} + \mu_{xy}^2/\mu_{yy}) + q_0^2k^2 \sin^2\phi[\mu_{xx}(1 - \mu_{zz}/\mu_{yy}) + \mu_{xy}^2/\mu_{yy}] \tag{17}$$

with $q_0^2 = \varepsilon_p\omega^2/c^2$ and assuming that there is no wave in the negative-y direction. For a given frequency ω, equation (15) clearly has two solutions for k_s because the magnetic crystal is birefringent and two transmitted waves propagate in the medium. Consequently this gives two reflected waves. One propagates with the same polarization as the incident wave (s to s reflection) while the other propagates with orthogonal or p polarization (s to p reflection). If we write k_s^+ and k_s^- as the two solutions of equation (15), $\boldsymbol{E}$ and $\boldsymbol{H}$ in the medium are given by

$$E_z/E_x = \lambda_\pm \qquad Ey/E_z = -(k_s^{\pm 2} - k^2 \sin^2\phi)^{-1/2}k \sin\phi \tag{18}$$

$$H_y/H_x = \alpha_\pm \qquad H_x/H_z = \beta_\pm \qquad H_z/E_x = \sigma_\pm/\mu_0\omega \tag{19}$$

where

$$\alpha_\pm = (k_s^{\pm 2} - \mu_{xx}q_0^2)/(\mu_{xy}q_0^2) \tag{20}$$

$$\beta_\pm = \frac{k_s^{\pm 2} - \mu_{zz}q_0^2 - k^2 \sin^2\phi}{(k_s^{\pm 2} - k^2 \sin^2\phi)^{1/2}k \sin\phi\alpha_\pm} \tag{21}$$

$$\lambda_\pm = \frac{\beta_\pm(k_s^{\pm 2} - k^2 \sin^2\phi)^{1/2}}{\alpha_\pm\beta_\pm k \sin\phi - (k_s^{\pm 2} - k^2 \sin^2\phi)^{1/2}} \tag{22}$$

$$\sigma_{\pm} = \frac{q_0^2}{\alpha_{\pm}\beta_{\pm}k\sin\phi - (k_s^{\pm 2} - k^2\sin^2\phi)^{1/2}}. \tag{23}$$

Using the field ratios given by equations (18) and (19), we finally obtain the electric and magnetic components of the transmitted waves:

$$\boldsymbol{E}_{\pm} = (t_{\pm}E_0)[1, -(k_s^{\pm 2} - k^2\sin^2\phi)^{-1/2}\lambda_{\pm}k\sin\phi, \lambda_{\pm}] \tag{24}$$

$$\boldsymbol{H}_{\pm} = (t_{\pm}\sigma_{\pm}E_0/\mu_0\omega)[\beta_{\pm}, \alpha_{\pm}\beta_{\pm}, 1] \tag{25}$$

where t_+ and t_- represent the transmission coefficients for both waves.

In the air gap ($-d < y < 0$) we have two downward propagating waves of wave vector $\boldsymbol{k}_d = (0, \mathrm{i}\kappa_0, k_\parallel)$ and two upward waves of wave vector $\boldsymbol{k}_u = (0, -\mathrm{i}\kappa_0, k_\parallel)$ with $\kappa_0 = (\varepsilon_p\sin^2\phi - \varepsilon_0)^{1/2}\omega/c$. For the down waves, the electric and magnetic fields are given by $(t_1E_0, 0, 0)$ and $(t_1E_0/\mu_0\omega)(0, k_\parallel, -\mathrm{i}\kappa_0)$ for s to s polarization and by $(t_2E_0)(0, \mathrm{i}k_\parallel/\kappa_0, 1)$ and $(t_2E_0/\mu_0\omega)(\kappa_2, 0, 0)$ for s to p polarization. These should be multiplied by the phase factor $\exp(\mathrm{i}(\mathrm{i}\kappa_0 y + k_\parallel z - \omega t))$ and the transmission coefficients are denoted by t_1 and t_2 with $\kappa_2 = -\mathrm{i}(k_\parallel^2 - \kappa_0^2)/\kappa_0$. The electric and magnetic fields of the up waves for both polarization can be obtained from those of the down waves by making the replacements $t_1 \to T_1, t_2 \to T_2, \kappa_0 \to -\kappa_0$ and $\kappa_2 \to -\kappa_2$.

We can now write down the electric and magnetic fields of the first reflected wave (s to s polarization) at the $y = -d$ interface with wave vector $(0, -k_\perp, k_\parallel)$ as $(r_{ss}E_0, 0, 0)$ and $(r_{ss}E_0/\mu_0\omega)(0, k_\parallel, k_\perp)$. For the second or p polarized wave, we have $(r_{sp}E_0)(0, k_\parallel/k_\perp, 1)$ and $(r_{sp}E_0/\mu_0\omega)(-\kappa_1, 0, 0)$ with $\kappa_1 = k/\cos\phi$. The phase factors for both waves are given by $\exp(\mathrm{i}(-k_\perp y + k_\parallel z - \omega t))$. In these expressions r_{ss} and r_{sp} denote the reflection coefficients for s to s and s to p polarization, respectively. The computed reflectivities are taken as the square moduli of these coefficients.

The electromagnetic boundary conditions for the tangential components of the electromagnetic fields at $y = -d$ and $y = 0$ lead to eight linear equations in the reflection coefficients r_{ss} and r_{sp} and six transmission coefficients t_1, t_2, T_1, T_2, t_+ and t_-. After some algebra we finally obtain the reflectivities given by

$$R_{ss} = |r_{ss}|^2 = \left|\frac{(k_\perp - \mathrm{i}\kappa_0)\mathrm{e}^{\kappa_0 d} + (k_\perp + \mathrm{i}\kappa_0)h_s\mathrm{e}^{-\kappa_0 d}}{(k_\perp + \mathrm{i}\kappa_0)\mathrm{e}^{\kappa_0 d} + (k_\perp - \mathrm{i}\kappa_0)h_s\mathrm{e}^{-\kappa_0 d}}\right|^2 \qquad \text{(s–s reflection)} \tag{26}$$

and

$$R_{sp} = |r_{sp}|^2 = \left|\frac{2g_sk_\perp(\mathrm{e}^{\kappa_0 d} + f_s\mathrm{e}^{-\kappa_0 d})}{(k_\perp + \mathrm{i}\kappa_0)\mathrm{e}^{\kappa_0 d} + (k_\perp - \mathrm{i}\kappa_0)h_s\mathrm{e}^{-\kappa_0 d}}\right|^2 \qquad \text{(s–p reflection)} \tag{27}$$

where

$$f_s = \left(\frac{\kappa_2 + \kappa_1}{\kappa_2 - \kappa_1}\right)\exp(2\kappa_0 d) \tag{28}$$

$$g_s = \frac{2\mathrm{i}\kappa_0(\lambda_+\beta_-\sigma_- - \lambda_-\beta_+\sigma_+)}{(1 + f_s)\Delta_s - 2\kappa_2[\lambda_-(\mathrm{i}\kappa_0 - \sigma_+) - \lambda_+(\mathrm{i}\kappa_0 - \sigma_-)]} \tag{29}$$

$$\Delta_s = (\mathrm{i}\kappa_0 - \sigma_+)(\lambda_-\kappa_2 + \beta_-\sigma_-) - (\mathrm{i}\kappa_0 - \sigma_-)(\lambda_+\kappa_2 + \beta_+\sigma_+) \tag{30}$$

and

$$h_s = [2\mathrm{i}\kappa_0(\lambda_-\kappa_2 - \lambda_+\kappa_2 + \beta_-\sigma_- - \beta_+\sigma_+) + 2g_s\kappa_2(\sigma_- - \sigma_+) - \Delta_s]/\Delta_s. \tag{31}$$

Finally, we consider similar calculations for incident p polarization. Expressions for the reflectivities can be derived as before. The results are given by

$$R_{pp} = |r_{pp}|^2 = \left| \frac{(\kappa_1 - \kappa_2)e^{\kappa_0 d} + (\kappa_1 + \kappa_2)h_p e^{-\kappa_0 d}}{(\kappa_1 + \kappa_2)e^{\kappa_0 d} + (\kappa_1 - \kappa_2)h_p e^{-\kappa_0 d}} \right|^2 \qquad \text{(p–p reflection)} \tag{32}$$

and

$$R_{ps} = |r_{ps}|^2 = \left| \frac{2g_p\kappa_1(e^{\kappa_0 d} + f_p e^{-\kappa_0 d})}{(\kappa_1 + \kappa_2)e^{\kappa_0 d} + (\kappa_1 - \kappa_2)h_p e^{-\kappa_0 d}} \right|^2 \qquad \text{(p–s reflection).} \tag{33}$$

The quantities appearing in equations (32) and (33) are now

$$f_p = \left(\frac{i\kappa_0 + k_\perp}{i\kappa_0 - k_\perp} \right) \exp(2\kappa_0 d) \tag{34}$$

$$g_p = \frac{2\kappa_2(\sigma_+ - \sigma_-)}{(1 + f_p)\Delta_p + 2i\kappa_0(\lambda_-\kappa_2 - \lambda_+\kappa_2 + \beta_-\sigma_- - \beta_+\sigma_+)} \tag{35}$$

$$\Delta_p = -\Delta_s \tag{36}$$

and

$$h_p = (2\kappa_2[\lambda_+(i\kappa_0 - \sigma_-) - \lambda_-(i\kappa_0 - \sigma_+)] + 2i\kappa_0 g_p(\lambda_-\beta_+\sigma_+ - \lambda_+\beta_-\sigma_-) - \Delta_p)/\Delta_p. \tag{37}$$

We should mention at this point that it is necessary to include a damping parameter Γ in the calculation of the ATR spectra and we simply do this by the replacement $\omega \to \omega + i\Gamma$.

To illustrate some numerical implications of the ATR formulae (26) and (27) and (32) and (33) for layered antiferromagnets, we present in figures 6 and 7 some ATR curves for surface polariton modes of NiO with dispersion curves already shown in figures 2 and 3. All spectra may be understood by reference to the scan line for $\phi = 42°$ and $\varepsilon_p = 11.56$ (Si), as drawn in figures 2 and 3. These are plotted for a moderate value of damping $\Gamma = 0.05$ cm^{-1}, which is typical of a good crystal of FeF_2 [1, 2] at low temperature, and a spacing $d = 1$ μm between prism and sample which is chosen to give strong surface mode dips. We also see broad dips which are usually attributed to overcoupling due to small spacing that gives rise to distorted surface mode lines and accordingly introduces the loss of energy to bulk polaritons [3].

Figure 6 shows the ATR curves of NiO for $H_0 = 3$ T with the scan line drawn in figure 3 and linewidth of the order of 0.2–0.3 cm^{-1}. As expected, spectra with the complete set of polarization combination (s–s, s–p, p–p and p–s) are produced as a result of the complicated polarization of the surface polariton fields. In all sets of curves we have made use of the tensor element μ_{zz} derived from an h/b analysis (curves with label a) and a conventional analysis (curves with label b). These clearly display the shifted frequency of the surface polariton mode, indicated by the two arrows with a difference in position by about 1 cm^{-1}, which directly originate from the difference between the two expressions for μ_{zz} and consequently should be open to experimental test. We may also note that the appearance of weak s to p and p to s reflection as given by equations (27) and (33) is a distinctive characteristic of the ATR spectra. We find that the p to s reflection is stronger than the s to p reflection by a factor of about four, as also found in FeF_2 [2].

To examine the effect of external field on the ATR spectra, we have plotted the calculated reflectivity for various values of H_0 in figure 7 where we have particularly made use of μ_{zz} derived from an h/b analysis. Three typical curves are drawn with $H_0 = 0, 3$ T and 7 T for all polarization combinations. We find that the curves shift slightly to lower frequency with increasing field.

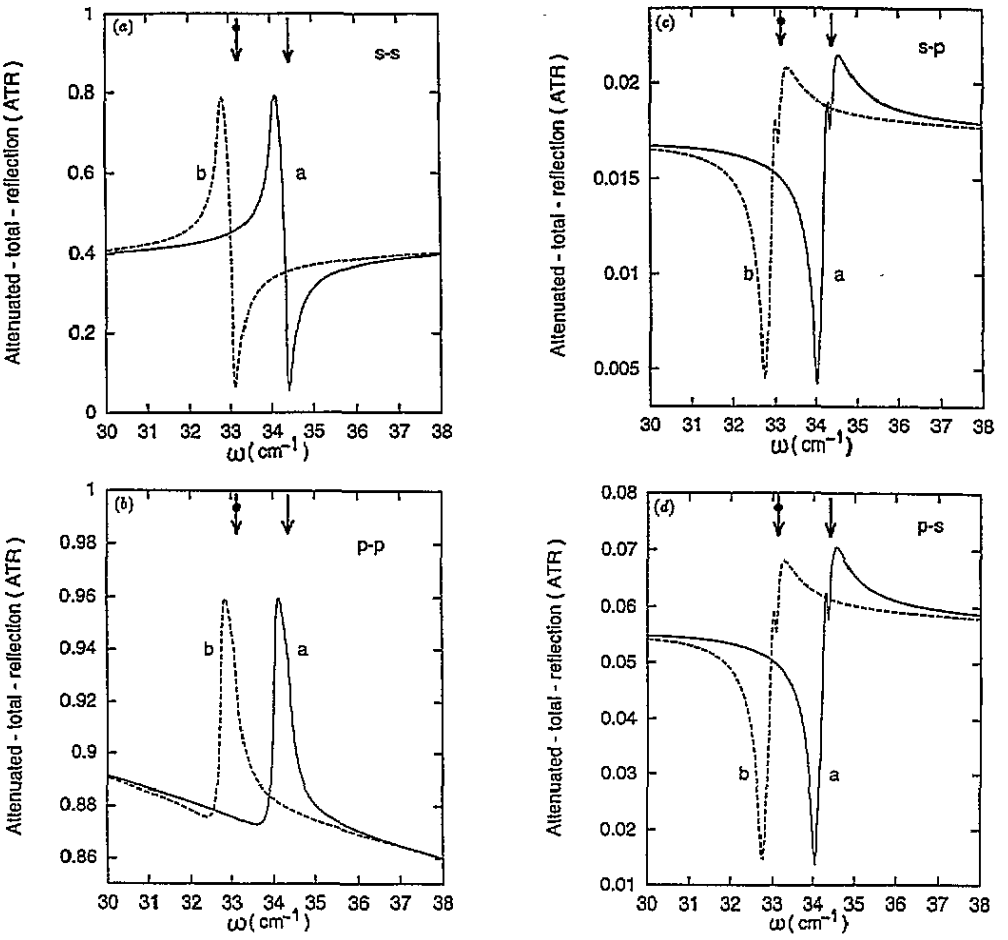

Figure 6. The calculated ATR spectra of surface polaritons on NiO whose dispersion curves are shown in figure 3 for (A) s to s, (B) p to p, (C) s to p and (D) p to s reflection. The surface polariton frequencies are indicated by the arrows, as depicted in figure 3, for both methods of constructing μ: (a) h/b method and (b) conventional method. Parameters in four sets of spectra are given by $H_0 = 3$ T, $\Gamma = 0.05$ cm^{-1}, $d = 1$ μm, $\phi = 42°$ and $\varepsilon_p = 11.56$.

The other main distinction between the ATR spectra presented here and those reported in [9] is the scale of the frequency scan for available field H_0 in a laboratory. In the previous work [9], the frequency scale of the ATR spectra in s polarization is set by ω_+ given by (3) which is of the order of up to 10 cm^{-1} for a modest value of H_0. It is unfortunately at the low end of the range that would be accessible to Fourier transform FIR spectroscopy. On the other hand, the frequency range of the ATR curves in this paper is scaled by the higher-mode frequency, either ω_- or ω_d, which is in the FIR region more easily accessible to the instrument. Finally, it is worth mentioning for NiO that the antiferromagnetic resonance (AFMR) frequency has recently been investigated by Raman scattering [15] and the lower mode (ω_+) by Brillouin scattering [16].

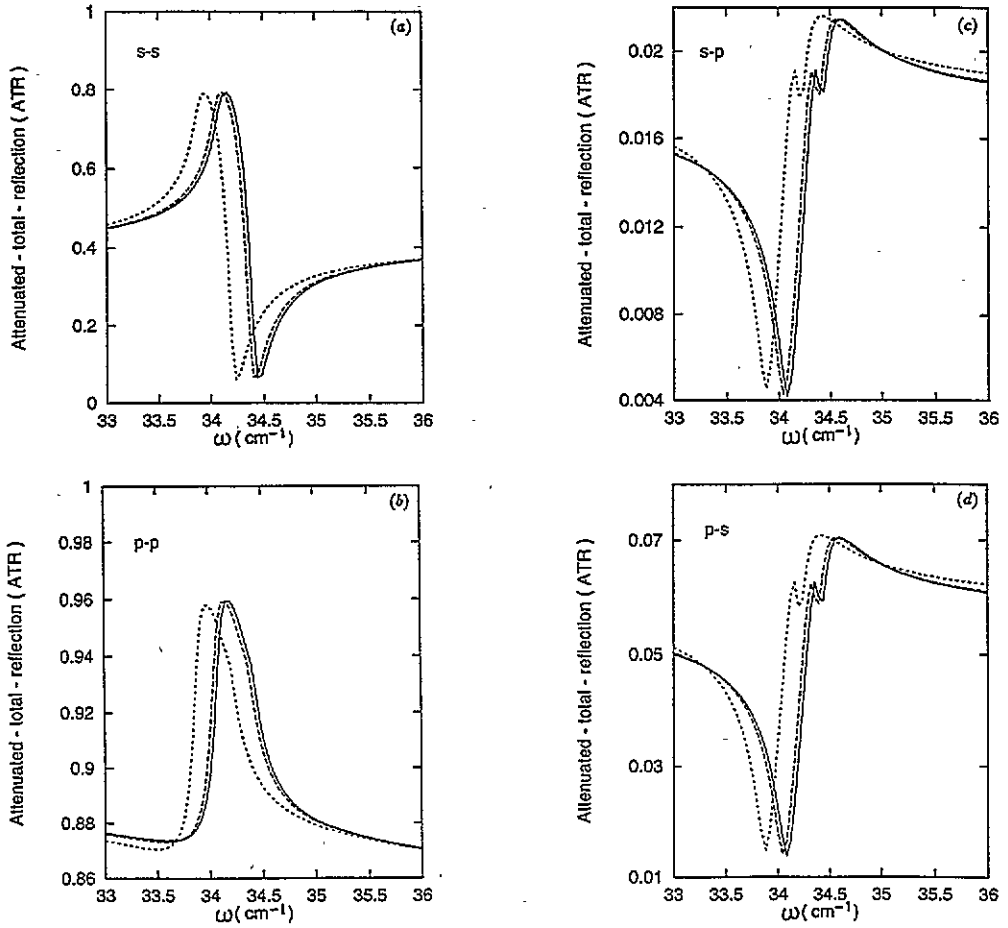

Figure 7. The field-dependent ATR spectra of surface polaritons on NiO whose dispersion curves are obtained in the h/b method. Polarization combinations are (a) s to s, (b) p to p, (c) s to p and (d) p to s with $H_0 = 0$ (solid lines), $H_0 = 3$ T (dashed lines) and $H_0 = 7$ T (dotted lines). Other parameters as quoted in figure 6.

4. Conclusions

In this paper we have given a full theoretical discussion for the surface polaritons (section 2) and ATR spectra (section 3) of layered antiferromagnets with equilibrium orientation of the sublattice moments shown in figure 1. The applied magnetic field is parallel to the surface of the sample and to the propagation direction. The theory is then applied to the specific case of NiO. There has recently been some uncertainty [4] about the correct means of determining the rf magnetic permeability tensor of this material. The two methods, which we refer to as the conventional and the h/b methods, disagree only over the correct form of μ_{zz}. In contrast to our previous work [9] for the Voigt geometry, the main question that is addressed in this paper is how the difference between the two expressions for μ_{zz} can be tested directly by an experiment aimed specifically at the surface polaritons; we show the dispersion and ATR curves of NiO.

Figures 3 and 6 are the most important results of this work. They show that the surface polariton dispersion curves obtained from relation (13) clearly display the shift due to μ_{zz};

that is, both curves are markedly separated in the ω–q plane with a difference in frequency of about 1 cm^{-1}. Using equations (26) and (27) and (32) and (33), the computed ATR spectra are shown in figure 6 which provide direct experimental probes for resolving the basic question mentioned before. Previous experience on FIR spectroscopy of magnetic features [1, 2] suggests that the ATR dips should be readily detectable.

In addition, our numerical results for NiO reveal for the first time the existence of the bona fide surface polariton and generalized surface modes in a magnetic system, like those found many years ago for surface magnetoplasmons of a semiconductor [11, 14]. We believe that the independent experimental observation of these modes, apart from FIR ATR spectroscopy, should be possible; for example, using modified ATR ellipsometry [17], Brillouin light scattering (BLS) [18–21] or Raman scattering. In reflection ellipsometry, both modes would certainly have different ellipsometric parameters Ψ and Δ due to the fact that they have different states of polarization. For example, the sign change in these parameters as the mode evolves from surface polariton to generalized surface wave would be interesting since it has already given a qualitative distinction between the two waves. Finally, we may note that some recent BLS studies have observed generalized surface modes and pseudosurface modes in PbTe [18], GaAs [19–21] and InSb [21].

Acknowledgments

KA acknowledges financial support from Proyek PS2PT DIKTI DEPDIKBUD (Bank Dunia XXI) Indonesia. We have benefited from helpful discussions with Bob Camley (Colorado Springs), and Terry Parker and Farag Elmzughi (Essex).

References

[1] Brown D E, Dumelow T, Parker T J, Abraha Kamsul and Tilley D R 1994 *Phys. Rev.* B **49** 12266
[2] Abraha Kamsul, Brown D E, Dumelow T, Parker T J and Tilley D R 1994 *Phys. Rev.* B **50** 6808
[3] Cottam M G and Tilley D R 1989 *Introduction to Surface and Superlattice Excitations* (Cambridge: Cambridge University Press)
[4] Stamps R L, Camley R E, Nortemann F C and Tilley D R 1993 *Phys. Rev.* B 48 15740
[5] Raj N and Tilley D R 1987 *Phys. Rev.* B **36** 7003
[6] Almeida N S and Mills D L 1988 *Phys. Rev.* B **38** 6698
[7] Almeida N S and Tilley D R 1991 *Phys. Rev.* B **43** 11145
[8] Abraha Kamsul and Tilley D R 1994 *Infrared Phys. Technol.* **35** 681
[9] Abraha Kamsul and Tilley D R 1995 *J. Phys.: Condens. Matter* **7** 2717
[10] Hutchings M T and Samuelsen E J 1972 *Phys. Rev.* B **6** 3447
[11] Wallis R F 1982 *Electromagnetic Surface Modes* ed A D Boardman (New York: Wiley)
[12] Landau L D and Lifshitz I M 1984 *Electrodynamics of Continuous Media* 2nd edn (Oxford: Pergamon)
[13] Camley R E 1987 *Surf. Sci. Rep.* **7** 103
[14] Kaplan H, Palik E D, Kaplan R and Gammon R W 1974 *J. Opt. Soc. Am.* 64 1551
[15] Lockwood D J, Cottam M G and Baskey J H 1992 *J. Magn. Magn. Mater.* **104–107** 1053
[16] Grimsditch M, Kumar Sudha and Goldman R S 1994 *J. Magn. Magn. Mater.* **129** 327
[17] Burshta I I, Venger E F and Zavadskii S N 1994 *Surf. Sci.* **301** 399
[18] Aleksandrov V V, Velichkina T S, Vorob'ev P G, Potapova Y B and Yakovlev I A 1993 *Sov. Phys.–JETP* **76** 1085
[19] Carlotti G, Fioretto D, Giovannini L, Nizzoli F, Socino G and Verdini L 1992 *J. Phys.: Condens. Matter* **4** 257
[20] Aleksandrov V V, Velichkina T S, Potapova Y B and Yakovlev A 1992 *Sov. Phys.– JETP* **75** 1018
[21] Aleksandrov V V and Potapova Y B 1992 *Solid State Commun.* **84** 401